# Elemental anion thermal injection synthesis of nanocrystalline marcasite iron dichalcogenide FeSe$_2$ and FeTe$_2$†

Ebin Bastola, Khagendra P. Bhandari, Anthony J. Matthews, Niraj Shrestha and Randy J. Ellingson*

We report a hot-injection colloidal method for the synthesis of nanocrystalline (NC) iron diselenide (FeSe$_2$), and iron ditelluride (FeTe$_2$) derived from iron(II) bromide as the iron (Fe) precursor. These highly crystalline iron chalcogenides are synthesized by injecting elemental selenium (Se) or tellurium (Te), complexed with oleylamine, into a reaction flask containing the iron precursor. NC FeSe$_2$ and FeTe$_2$ films have been characterized by using X-ray diffraction (XRD), scanning electron microscopy (SEM), and Raman spectroscopy. Both FeSe$_2$ and FeTe$_2$ NC particles exhibit marcasite phase with orthorhombic crystal structure. The as-synthesized NC FeSe$_2$ and FeTe$_2$ show irregular shapes with consistent stoichiometric ratio. In addition, we discuss these iron chalcogenides with regard to their thin film electronic properties including sheet resistance, resistivity, majority carrier type, and their possible device applications.

## Introduction

Semiconductor nanocrystalline materials offer many promising properties for electronic and photonic applications.[1,2] Potentially simplified material preparation and solution-sourced thin film processing from nanocrystals enable consideration of inexpensive inkjet or screen printing on rigid or flexible substrates. In many cases, solution-sourced nanocrystals can be deposited in thin film form at room temperature to yield excellent optoelectronic performance.[3–5] Semiconductor nanocrystals and nano-composites have great potential in the field of photovoltaics (PV),[6–8] medicine,[9] light emitting devices,[10,11] and photocatalysis.[12] Researchers routinely search for alternative materials to improve upon those presently used commercially, in an effort to reduce material input or manufacturing cost, enhance performance, or reduce undesired environmental costs. For example, several studies in recent years have demonstrated the possible application of earth abundant chalcogenides[13–15] which can reduce toxicity in photovoltaic and other optoelectronic devices. While much attention has been drawn recently to the understanding and development of iron pyrite (FeS$_2$), here we discuss the colloidal synthesis and properties of nanocrystalline (NC) iron diselenide (FeSe$_2$) and iron ditelluride (FeTe$_2$), with grain sizes on the order of or less than 100 nm.

*Wright Center for Photovoltaics Innovation and Commercialization, School for Solar and Advanced Renewable Energy, Department of Physics and Astronomy, The University of Toledo, 2801 W. Bancroft Street, Toledo, Ohio 43606, USA. E-mail: randy.ellingson@utoledo.edu*

† Electronic supplementary information (ESI) available. See DOI: 10.1039/c6ra06351a

Several authors have reported the synthesis of iron dichalcogenides by methods including high temperature solid state reaction,[16] high temperature and high pressure,[17] molecular precursor solution synthesis,[18] ultrasonic chemical synthesis,[19] and metal organic chemical vapor deposition (MOCVD).[20] However, the most commonly reported techniques for synthesizing FeSe$_2$ and FeTe$_2$ are hydrothermal,[21–23] and solvothermal methods.[24] Though the wet-chemical method is an easy route, very few reports exist for iron dichalcogenide NC synthesis by this approach. Iron dichalcogenides, especially iron pyrite (FeS$_2$), have been studied for many decades with interest in their applications to photovoltaics and other energy conversion processes. Several groups have studied iron pyrite as the potential absorbing layer in solar cells, with limited success owing to the material's tendency for very high ionized defect densities and strongly limited photovoltage.[25,26] Our previous work has shown that FeS$_2$ NCs can serve as an interface material for a low barrier back contact to CdTe solar cells.[5] Other iron dichalcogenides, FeSe$_2$, and FeTe$_2$, although their fabrication using colloidal methods has slowly begun, have not been well explored for possible applications as opto-electronic materials. Although both materials have been prepared at elevated temperature in the cubic pyrite structure, they readily form the marcasite orthorhombic structure. Early studies indicated that the marcasite forms of FeSe$_2$ and FeTe$_2$ are narrow band gap semiconductors with complicated temperature-dependent transport properties.[27] In addition, FeSe$_2$ and FeTe$_2$ materials possess magnetic properties,[22,23,28] and based on a theoretical study, FeSe$_2$ offers distinct promise as a thermoelectric material.[29] Furthermore, authors have reported the performance of solution-processed FeSe$_2$ thin films as counter electrodes with

performance comparable to the conventional platinum electrodes in dye-sensitized solar cells.[30,31] Li *et al.* have reported the synthesis of $FeSe_2$ nanoparticles exhibiting laminar morphology using triethylene glycol as solvent, triethyleneterramine as an assisting agent, and polyvinylpyrrolide as a dispersing agent.[32] Recently, Qin *et al.* have also reported hot-injection synthesis of $FeSe_2$ NCs by using iron(II) acetylacetonate, and elemental selenium,[33] and recent work reported the synthesis of 30–100 nm $FeSe_2$ NCs in the presence of ethylenediamine.[34] However, these authors have not described the dependence of growth time on particle shape and size, and on the thin film electronic characteristics. Similarly, very few solution based methods have been reported to prepare $FeTe_2$ nanoparticles. Oyler *et al.* have reported a solution based method to grow nanosheets of iron chalcogenides (FeSe, FeTe, Fe(Se,Te), and $FeTe_2$),[35] and Zhang *et al.* have synthesized $FeTe_2$ NCs by dissolving elemental Te and the iron(II) complex $Na_2$[-Fe(EDTA)] in aqueous solution at 140 °C.[36] The synthesis of NC $FeTe_2$ by hot-injection colloidal method using iron(II) bromide as Fe source, elemental Te, and 1,2-hexanediol as surfactants, to the best of our knowledge, has not been previously reported.

We present a hot-injection colloidal synthesis of NC $FeSe_2$, and $FeTe_2$ using iron(II) bromide[37] as the cation precursor, and elemental Se and Te as anion sources. Marcasite phase NCs with orthorhombic crystal structure are grown in the temperature range of 200 °C to 340 °C using 1,2-hexanediol as the surfactant to enhance the yield of NC $FeX_2$ (X = Se, Te) control of nucleation and growth. Further, the shape and size of the NCs depend on the growth durations, and here, the influence of reaction time on shape and size of the NCs has been investigated by varying the growth interval following anion precursor injection.

# Experimental

### Chemicals

Materials utilized include iron(II) bromide ($FeBr_2$, anhydrous 99.9%; Alfa-Aesar), oleylamine (OLA, 70%; Sigma-Aldrich, or S.A.), 1,2-hexanediol (S.A.), Se powder (S.A.), methanol ($CH_3OH$, 99.5%; S.A.), chloroform ($CHCl_3$; Fisher-Scientific), Te powder (anhydrous, 99.9%; S.A.), and trioctylphosphine (TOP, S.A.). The elemental Se and Te powders were stored in a nitrogen environment glove box to avoid the formation of any hazardous compounds such as $H_2Se$ and $H_2Te$ gases. All chemicals are used as obtained without further purification, and the reactions were performed under nitrogen atmosphere.

### Synthesis procedure

Iron dichalcogenide ($FeSe_2$ and $FeTe_2$) syntheses were done under nitrogen atmosphere using standard Schlenk line technique. The typical method used to synthesize $FeSe_2$ NCs was similar to that reported previously for iron pyrite ($FeS_2$) NCs.[37] Iron(II) bromide ($FeBr_2$) was the source of $Fe^{2+}$ ions, and elemental Se was used as the $Se_2^{2-}$ anion source. In a three neck flask, 0.5 mmol $FeBr_2$, 0.4 mL 1,2-hexanediol, and 10 mL OLA were taken; the three-neck flask was evacuated and purged with

nitrogen, repeated twice, to remove residual air. The mixture was then heated at 170 °C for 2 hours to dissolve $FeBr_2$ into OLA. To prepare the Se source, 3 mmol Se was mixed with 10 mL OLA in a vial in the glove box. The Se mixture was sonicated for ∼15 minutes, and heated at ∼200 °C until the Se powder was completely dissolved in OLA. To support temperature control and stability during NC nucleation, the dissolved Se in OLA was held at 200 °C until the time of injection into the reaction flask, and the mixture was held at the same temperature for the growth of NCs over different time durations. After the desired growth time of NCs, the heating mantle was removed and the flask was allowed to cool down to room temperature. The NCs thus synthesized were cleaned by centrifugation at 2400 × $g$ in chloroform with methanol as the non-solvent, and the purified NCs were stored dry in an $N_2$ glove box for further characterization. Similarly, to synthesize $FeTe_2$ NCs, the $Fe^{2+}$ source in the reaction flask was prepared identically as described above, and the Te source was prepared by adding 3 mmol of elemental Te to 3 mL TOP. The Te source was sonicated ∼15 minutes to dissolve the Te, and then ∼7 mL OLA was added into it. The mixture was then injected to the reaction flask at 300 °C, and heated for different time durations to study the growth patterns of NCs at the same temperature. The $FeTe_2$ NCs were purified as described above. For both $FeSe_2$ and $FeTe_2$ syntheses, the temperature was varied to determine optimal conditions for high yield and crystallinity of NC marcasite.

### Thin film preparation

Nanocrystalline thin films were prepared using layer by layer drop-casting onto a sodalime glass substrate in the fume hood. For this, $FeX_2$ NCs were dissolved in chloroform at a concentration of ∼6 mg mL$^{-1}$. To disperse the NCs fully in the solvent, the solution was sonicated with Digital Ultrasonic Cleaner Model PS-10A, and ultrasonic power of 70 W.

### Characterization

The X-ray diffraction pattern of the $FeX_2$ films were taken using a Rigaku Ultima III X-ray Diffractometer fitted with small angle X-ray Scattering (SAXS) at 40 kV accelerating voltage, and 44 mA current. Scherrer analysis was used to determine the average grain sizes for each sample. A Hitachi S-4800 UHR scanning electron microscope (SEM) was used to take the SEM images of the sample. Energy dispersive X-ray spectroscopy (EDS) was measured at an accelerating voltage of 20 kV to study the composition/stoichiometry of the materials. Optical absorption spectra of the NC solutions and the films were taken using a PerkinElmer Lambda 1050 UV/Vis/NIR spectrophotometer. To study the Raman vibrational peaks of the material, a Jobin Yvon Horiba confocal Raman spectrometer fitted with HeNe laser source of wavelength 632.8 nm was employed. A Lucas 4 Probe was used to determine the sheet resistance of the thin films, and film thickness was measured using a Dektak 1050 Profilometer. Hot probe measurements employed a lab-constructed apparatus to determine the sign of the Seebeck coefficient as an indication of majority carrier type in $FeX_2$ thin films.[38]

# Results and discussion

## Crystal structure and phase analysis

Fig. 1(a) displays the X-ray diffraction (XRD) pattern of as-synthesized NC FeSe$_2$. The sharp peaks in the XRD pattern confirms that the material synthesized was highly crystalline in nature, and indicates that the NC FeSe$_2$ exhibit orthorhombic crystal structure ($a \neq b \neq c$, $\alpha = \beta = \gamma = 90°$). The crystal structure belongs to the space group $P_{nnm}$ (58), with $a = 0.4799$ nm, $b = 0.5777$ nm, $c = 0.3576$ nm.[39] Hence, the synthesized NC FeSe$_2$ exists in marcasite phase with orthorhombic crystal structure. The vertical lines in the graph are the reference lines of the standard FeSe$_2$ marcasite material obtained from the MDI JADE software (PDF 97-004-2041). With no evident discrepancy, these vertical lines match the peaks of the measured XRD of the synthesized sample which illustrates that these NCs maintain high phase purity.

Keeping the temperature of the Se precursor solution as close to 200 °C as possible, the Se solution was injected into the reaction flask containing the Fe precursor solution. The NC materials obtained at growth temperatures of 200 °C, 240 °C, 280 °C and 320 °C were investigated. Immediately after the injection of the Se precursor, the temperature of the reactants solution dropped to the range of 185 °C (for 200 °C starting point) to 240 °C (for 320 °C starting point), and rapidly returned to the initial temperature. In all these cases, NC FeSe$_2$ so obtained are of marcasite phase with orthorhombic crystal structure. Interestingly, the properties of the NC product are independent of the injection temperature within this reaction temperature range. The XRD pattern of all these samples are shown in Fig. SF1 in the ESI.† The XRD pattern presented here are similar to the previous reports obtained from hydrothermal and solvothermal methods.[23,24] The XRD peaks of NC FeSe$_2$ samples match, independent of reaction temperature, and the sharp peaks of the pattern confirm that these materials are highly crystalline in nature. The only discernible temperature-dependent property of the reaction we note was that yield improved for 240 °C and higher growth temperatures.

The average grain sizes of the NC FeSe$_2$ were estimated by using Debye–Scherrer analysis given by, $D_\mathrm{p} = \dfrac{K\lambda}{\beta \cos \theta}$ where $D_\mathrm{p}$ is the grain size, $K$ is the shape factor usually taken as close to unity, $\lambda$ is the wavelength of the X-ray used, $\beta$ is the full width at half maximum (FWHM) in radians, and $\theta$ is the Bragg's diffraction angle. Based on the XRD pattern presented in Fig. SF1 in the ESI,† the Scherrer-analysis was completed to estimate the grain size of the FeSe$_2$ synthesized at different temperature, and the results are summarized in the Table 1. For this calculation, $K = 0.94$, and $\lambda = 0.154059$ nm were used in the equation, $\beta$ was calculated by fitting each diffraction peak by Gaussian function and was corrected by using X-ray broadening ($0.08° = 1.4 \times 10^{-3}$ rad). The value of the grain size obtained from calculation is rounded to the nearest nanometer. The grain sizes of the FeSe$_2$ NCs synthesized in the temperature range of 200 °C to 320 °C are similar in spite of different reaction temperature. Grain size analysis of the XRD pattern indicates that the sizes of the synthesized FeSe$_2$ are still nanocrystalline in order, and the larger features in SEM imaging indicate coalescence.

Similarly, the XRD pattern of as-synthesized FeTe$_2$ also shows sharp peaks indicating that the material is highly crystalline, as shown in Fig. 1(b). The XRD pattern corresponds with the pattern of iron ditelluride (PDF 97-063-3879) of the JADE software. These NC FeTe$_2$ belong to marcasite phase with orthorhombic crystal structure with $a = 0.5265$ nm, $b = 0.6265$ nm, $c = 0.3869$ nm, and the crystal structure belongs to space group $P_{nnm}$ (58).[40] In addition, these XRD patterns of NC FeTe$_2$ are similar to the XRD pattern reported previously.[23,35] As with the FeSe$_2$, the phase and crystal structure of FeTe$_2$ were found to be independent of the growth temperature in the range of 220 °C to 300 °C. However, the yield was found comparatively better at 300 °C than at 220 °C and 260 °C. FeTe$_2$ could be synthesized
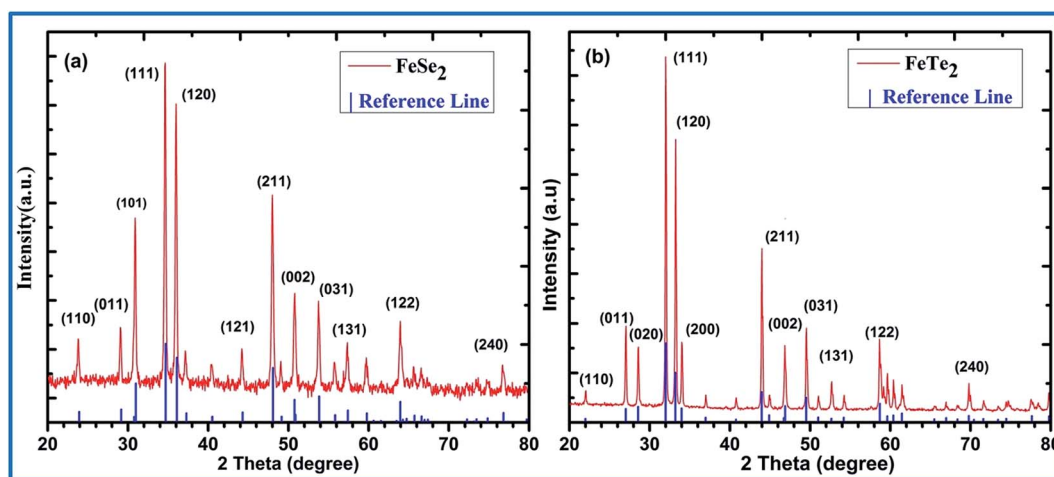


**Fig. 1** X-ray diffraction pattern of as-synthesized nanocrystalline (a) FeSe$_2$, and (b) FeTe$_2$. Both materials possess orthorhombic crystal structure, marcasite phase, and the sharp intensity peaks of the pattern indicate phase-pure crystalline material. The reference lines for FeSe$_2$ and FeTe$_2$ materials are PDFs # 97-004-2041 and # 97-063-3879 obtained from MDI JADE software respectively.

**Table 1** Scherrer-analysis of NC FeSe$_2$ synthesized at different temperatures

| S.No. | Synthesis temperature (°C) | Grain size based on the peak at (nm) | | | | Average grain size ($D_p$) (nm) |
|---|---|---|---|---|---|---|
| | | (101) | (111) | (120) | (211) | |
| 1 | 200 | 67 | 58 | 62 | 47 | 59 ± 9 |
| 2 | 240 | 63 | 64 | 65 | 52 | 61 ± 6 |
| 3 | 280 | 59 | 64 | 62 | 48 | 58 ± 7 |
| 4 | 300 | 53 | 62 | 63 | 54 | 58 ± 5 |



**Fig. 2** Scanning electron microscopy (SEM) images of as-synthesized (a) and (b) FeSe$_2$ nanocrystals (c) and (d) FeTe$_2$ nanocrystals.

using only TOP to dissolve the Te powder, though the FeTe$_2$ yield clearly improved when OLA was added to TOP. The existence of OLA is expected to assist with elemental Te dissolution through binding by the amine group.[41,42] The XRD pattern of the NC FeTe$_2$ grown at different temperature are shown in the Fig. SF2 in ESI,† and the sharp peaks of these patterns again illustrate that the product exhibits excellent crystallinity independent of growth temperature. Similar to the NC FeSe$_2$, the Scherrer-analyses for FeTe$_2$ NCs synthesized at different temperatures were carried out on the XRD patterns presented in Fig. SF2 in ESI† and the results appear in Table 2 with average grain sizes from ∼78 to 100 nm.

### Surface morphology and EDS analysis

To study the surface morphology of FeSe$_2$, films were prepared by drop-casting onto sodalime glass substrates. The SEM images of the FeSe$_2$ film are shown in Fig. 2(a and b). The NC FeSe$_2$ films show flake-like surface morphology with feature sizes in the range of ∼150 nm to ∼1 μm. Qin et al. reported flower-like micron-sized FeSe$_2$ crystallites by hot-injection synthesis while Yuan et al. have reported flake-like particles 100 nm to 200 nm in diameter by a solvothermal method.[24,33] The EDS analyses of these NC thin films are shown in Table 3. The NC FeSe$_2$ is found to be nearly stoichiometric with Se to Fe atomic ratio 1.99 ± 0.03, and we find excellent stoichiometric reproducibility within different syntheses.

SEM images of FeSe$_2$ NCs synthesized with different growth durations such as 1 minute, 5 minutes, 15 minutes, and 30 minutes after the injection of Se precursor to the reaction flask at 240 °C are shown in Fig. SF3 (ESI†). We found that the yield of FeSe$_2$ for 1 minute growth duration was relatively low while other growth durations 5 minutes and higher produced

a similar improved yield. The NCs grown for longer durations show slightly larger average size than the NCs grown for 1 minute. Based on the SEM images, these NCs grown for different time intervals have very similar shape, and surface morphology. Here, all of the FeSe$_2$ NC products show the pure marcasite phase with orthorhombic crystal structure, and the ratio Fe to Se atoms is ∼1 : 2. Further, we did not observe any change in color of the FeSe$_2$ thin films during the characterization process indicating the films are stable in ambient conditions.

Similarly, FeTe$_2$ thin films were also prepared by using layer by layer drop-cast method, to investigate the morphology of the NC FeTe$_2$ thin films using SEM and EDS measurements. The SEM images of as-synthesized FeTe$_2$ are shown in Fig. 2(c and d). The feature sizes of the FeTe$_2$ thin films vary from ∼200 nm to ∼500 nm with apparently widely-varied crystalline shape. Zhang et al. have reported marcasite FeTe$_2$ synthesized by the hydrothermal route yielding shape-nonspecific nanoparticles[36] as well as nanorods.[43] Similar to FeSe$_2$, the NC FeTe$_2$ was also found to be close to stoichiometric where the average atomic ratio of Te to Fe atoms is 2.04 ± 0.03. In addition, SEM images of the NC FeTe$_2$ thin films resulting from injection and growth at 300 °C with different reaction time such as 1 minute, 5 minutes, 15 minutes, and 30 minutes are shown in the ESI, Fig. SF4.† The SEM image belonging to 1 minute growth time (SF4a†) is quite different than the rest of the SEM images. The XRD pattern of this 1 minute grown sample showed unidentified peaks in addition to the peaks of the orthorhombic crystal structure, and from the EDS measurement, Fe to Te atomic ratio was found to be close to 1 : 1. This indicates that the initial nucleation and growth within ∼1 minute growth time favors formation of a different crystalline structure, and that for FeTe$_2$ the marcasite phase forms after nucleation. These FeTe$_2$ NCs having longer growth time have a similar surface morphology as shown in Fig. SF4(b–d).† As was observed for the FeSe$_2$, the size of FeTe$_2$ NCs depends on growth time, with longer growth time yielding slightly larger NCs. Similar to FeSe$_2$ films, we did not

**Table 2** Scherrer-analysis of FeTe$_2$ NCs synthesized at different temperatures

| S.No. | Synthesis temperature (°C) | Grain size based on the peak at (nm) | | | | Average grain size ($D_p$) (nm) |
|---|---|---|---|---|---|---|
| | | (011) | (111) | (120) | (211) | |
| 1 | 240 | 102 | 109 | 100 | 89 | 100 ± 8 |
| 2 | 280 | 85 | 86 | 84 | 68 | 81 ± 8 |
| 3 | 300 | 83 | 79 | 79 | 73 | 78 ± 4 |
| 4 | 320 | 115 | 108 | 99 | 77 | 100 ± 17 |

**Table 3** EDS analysis of as synthesized FeSe$_2$ and FeTe$_2$. The instrumental error is estimated at ±3%

| FeSe$_2$ NCs | | FeTe$_2$ NCs | |
|---|---|---|---|
| Elements | Atomic% | Elements | Atomic% |
| Fe K | 33.54 | Fe K | 32.75 |
| Se L | 66.36 | Te L | 67.25 |

notice any change in color or smell on FeTe$_2$ thin films during the preparation, and characterization of this material indicating good stability of the materials. In addition, typical EDS measurement spectra are shown in Fig. SF5 of the ESI† for both NC FeSe$_2$ and FeTe$_2$ (Table 3).

## Raman spectroscopy

Fig. 3 shows the results of Raman spectroscopy measurements carried out using a 632.8 nm HeNe laser source to further characterize the NC FeSe$_2$ and FeTe$_2$ thin films. The FeSe$_2$ film shows distinct Raman active modes at 180 cm$^{-1}$, 220 cm$^{-1}$ and 256 cm$^{-1}$. Lutz and Müller measured Raman spectra for FeSe$_2$ marcasite, attributing peaks at 221 cm$^{-1}$ and 264 cm$^{-1}$ to A$_g$ and B$_{1g}$ Se–Se stretching modes, and a peak at 183 cm$^{-1}$ to a librational mode;[44] these peaks agree reasonably well with our measurements, and we note that the Raman laser excitation wavelengths differ slightly (632.8 nm in our case *vs.* 676.4 nm). These active vibrational peaks of Se–Se atoms closely agree with the peaks which have been previously reported for nanocrystalline FeSe$_2$.[24,33] We observe Raman peaks for NC FeTe$_2$ thin films at 119 cm$^{-1}$ and 137 cm$^{-1}$ and these peaks are attributed to the libration modes.[44] Interestingly, we did not clearly discern a peak at 155 cm$^{-1}$ due to the Te–Te stretching mode previously reported.[44] However, based on the evidence provided by the XRD, EDS, and Raman analyses, we conclude that the NC FeTe$_2$ synthesized here belong to marcasite phase with orthorhombic crystal structure.

## UV-Vis-NIR spectroscopy

The absorbance spectra of as-synthesized NC FeSe$_2$ dispersed in chloroform were taken using a Perkin Elmer Lambda 1050 spectrophotometer in the spectral region from 350 nm to 1500 nm. Although the theoretical value for the band gap of bulk FeSe$_2$ material has been reported to be 1 eV,[45] the reported experimental values vary more widely within the range of 1.03 to 1.24 eV.[24,32,46,47] A typical absorbance spectrum of NC FeSe$_2$ taken in chloroform as a solvent is given in the ESI, Fig. SF6(a).† Qin *et al.* have reported an absorption peak of FeSe$_2$ NCs at 1135 nm; however, they did not present a wide bandwidth measurement of absorption from UV to the NIR.[33] Unlike the report of Qin *et al.*, our optical absorption measurements of FeSe$_2$ NCs carried out in hexane, trichloroethylene, and in thin film form did not exhibit a clear peak. Instead, we observed a largely featureless spectrum for which optical extinction increased gradually with wavelength through most of the visible and the near-infrared region. As stated earlier, our NC FeSe$_2$
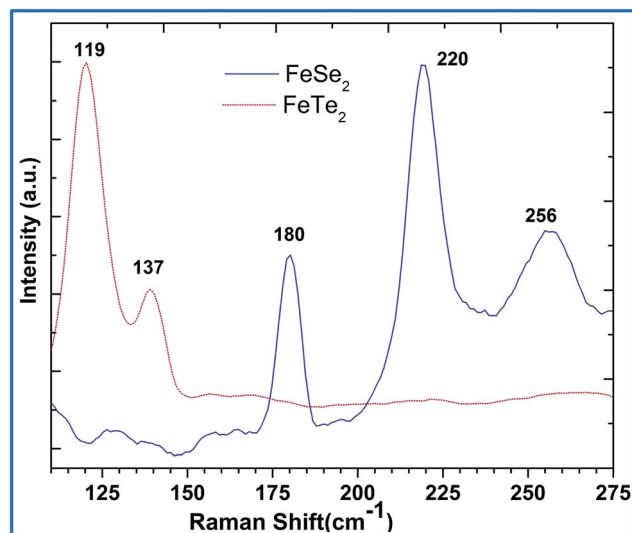


**Fig. 3** Raman spectroscopy measurement of as-synthesized NC FeSe$_2$ and FeTe$_2$ using 632.8 nm excitation from a HeNe laser.

range in size from ∼150 nm to ∼1 μm, with irregularly shaped NCs. Yuan *et al.* have reported an increase in absorbance as wavelength increases in FeSe$_2$ particles synthesized at 180 °C; their measured absorbance spectrum is almost identical for 220 °C growth temperature, and they show a broad optical absorption peak for FeSe$_2$ NCs synthesized by a solvothermal method at higher temperatures (260 °C, 300 °C).[24] We find non-zero absorption over the entire range we measured. Absorption in longer wavelength region is unexpectedly higher (SF6a†), similar to the UV-Vis-NIR spectra reported by Yuan *et al.* for FeSe$_2$ particles synthesized at 180 °C,[24] which indicates the presence of a high density of mid-gap defect states.

Similarly, the absorbance spectra of NC FeTe$_2$ dispersed in chloroform were measured in the wavelength range 350 nm to 2200 nm. However, we did not observe any absorption peaks in the selected wavelength range as shown in the ESI, Fig. SF6(b).† The nature of this absorption remained unchanged with respect to solvents used to disperse the NCs and also for the NC thin film. The reported band gap values of this material fall in the range of 0.2 to 0.5 eV.[27,48] Compared with iron pyrite FeS$_2$, the FeSe$_2$ and FeTe$_2$ NCs incorporate chalcogenides with increasing atomic radii, and hence the outer electrons ionize more readily indicating they possess more metallic character than sulfur. The reason behind the increase in absorbance in the IR region might be due to defect-induced generation of large free carriers populations (electrons and holes)[24] corresponding to semi-metallic behavior of the material.

## Electronic properties

The electronic properties of the as-synthesized FeSe$_2$ and FeTe$_2$ films were studied using thermal probe, and four point probe measurements, and the film thicknesses were measured using a Dektak profilometer. To find the majority carrier type for each material, we employed the thermal probe measurement method, which utilizes a simple two-probe test in which one

probe is heated to drive diffusion of free carriers. The basic experimental setup is quite similar to a system used to measure the Seebeck coefficient, though in the case of the thermal probe we are concerned only with the sign of the signal as a method to identify the majority carrier type. For thin films of both $FeSe_2$ and $FeTe_2$, the deflection in the voltmeter was opposite (negative) to that of the n-type silicon wafer (positive). Thus the majority charge carriers in as-synthesized $FeSe_2$ and $FeTe_2$ NCs films are holes, indicating that both of the marcasite NC iron dichalcogenide materials are p-type. Our typical as-synthesized $FeSe_2$ film of average thickness $\sim$6.2 μm shows an average sheet resistance of $\sim$3.0 × $10^4$ Ω □$^{-1}$, and the resistivity is 19.3 Ω cm. Similarly, in our typical $FeTe_2$ film with an average thickness of $\sim$5.3 μm shows a measured average sheet resistance value of $\sim$8.0 × $10^3$ Ω □$^{-1}$, corresponding to a resistivity of 4.1 Ω cm. The previously reported resistivity values for bulk $FeSe_2$ material fall in the range of 0.26–1 Ω cm (ref. 27, 47 and 49) and for $FeTe_2$ $\sim$ 0.015 Ω cm.[50] Our measured values are significantly higher, which we explain based on the presence of long chain organic molecules like 1,2-hexanediol, and oleylamine, in as-synthesized $FeSe_2$ and $FeTe_2$ NCs. For comparison, the resistivity of as-synthesized iron pyrite $FeS_2$ NCs (containing the tri-octylphosphine oxide (TOPO) molecules used in synthesis) for a typical film of average thickness 3.5 μm was $\sim$120 Ω cm, and after hydrazine treatment to remove TOPO surfactant molecules the resistivity decreased to $\sim$12 Ω cm.[37] Hence, these as-synthesized marcasite $FeSe_2$ and $FeTe_2$ NCs films are more conductive than as-synthesized iron pyrite $FeS_2$ NCs film. The comparison of the resistivity of these $FeSe_2$ and $FeTe_2$ thin films with $FeS_2$ films is made based on the (i) similar synthesis procedure using same iron precursor, (ii) similar thin film preparation method, and (iii) similar films thicknesses even though the particle feature sizes of NC $FeSe_2$ (or NC $FeTe_2$) are larger than $FeS_2$ NCs. Also, we note that in all cases the resistivity/conductivity of these $FeSe_2$ and $FeTe_2$ thin films does not reflect the intrinsic properties of the grains or crystals of these materials, but rather is expected to be dominated by the inter-grain transport. We have previously reported that $FeS_2$ NCs can serve as an effective back contact for CdTe solar cells;[5] however, we have as yet been unable to test these $FeSe_2$, and $FeTe_2$ marcasite NCs in a similar role. In principle, through improved surface control and film formation, these marcasite phase films which show improved conductivity may find a role in electronic materials. The reported narrow band gap energies for the marcasite Se and Te iron dichalcogenides do not suggest a role as a light-absorbing layer in highly efficient solar cells. While the decreased band gap energy suggests that any sustained photovoltage would be low, additional measurements are also needed to determine the band edge energetics, defect state distributions, and free carrier concentrations.

## Conclusion

The NC iron dichalcogenides of $FeSe_2$ and $FeTe_2$ have been successfully synthesized by hot-injection of elemental Se and Te, respectively, into a bromine-anion Fe precursor solution. For both $FeSe_2$ and $FeTe_2$, the as-synthesized NC particles have orthorhombic crystal structure, and are in marcasite phase with flower and flake like shape. Based on Raman spectroscopy, NC $FeSe_2$ shows active modes at 180 cm$^{-1}$, 220 cm$^{-1}$, and 256 cm$^{-1}$ while NC $FeTe_2$ shows modes at 119 cm$^{-1}$ and 137 cm$^{-1}$. The straightforward synthetic process described here enables additional discovery of NC $FeSe_2$ and $FeTe_2$ properties with applications in magnetic, electronic, and thermoelectric applications. These as-synthesized $FeSe_2$ and $FeTe_2$ films show p-type conductivity based on hot-probe measurement, and they exhibit relatively low conductivity due to the presence of long-chain hydrocarbon surfactant molecules. We measured unexpectedly weak and featureless optical absorption spectra. Although the reported narrow band gap of these materials indicate that they likely will not find success as absorber layers in photovoltaic devices, we are optimistic that the facile colloidal synthesis route to NC $FeSe_2$ and $FeTe_2$ materials demonstrated here will enable continued exploration of their properties and potential application in opto-electronic devices.

## References

1 H. Zhou, W.-C. Hsu, H.-S. Duan, B. Bob, W. Yang, T.-B. Song, C.-J. Hsu and Y. Yang, *Energy Environ. Sci.*, 2013, **6**, 2822–2838.

2 D. V. Talapin, J.-S. Lee, M. V. Kovalenko and E. V. Shevchenko, *Chem. Rev.*, 2009, **110**, 389–458.

3 C.-H. M. Chuang, P. R. Brown, V. Bulović and M. G. Bawendi, *Nat. Mater.*, 2014, **13**, 796–801.

4 V. Sukhovatkin, S. Musikhin, I. Gorelikov, S. Cauchi, L. Bakueva, E. Kumacheva and E. Sargent, *Opt. Lett.*, 2005, **30**, 171–173.

5 K. P. Bhandari, P. Koirala, N. R. Paudel, R. R. Khanal, A. B. Phillips, Y. Yan, R. W. Collins, M. J. Heben and R. J. Ellingson, *Sol. Energy Mater. Sol. Cells*, 2015, **140**, 108–114.

6 N. Kholmicheva, P. Moroz, U. Rijal, E. Bastola, P. Uprety, G. Liyanage, A. Razgoniaev, A. D. Ostrowski and M. Zamkov, *ACS Nano*, 2014, **8**, 12549–12559.

7 I. J. Kramer and E. H. Sargent, *Chem. Rev.*, 2014, **114**, 863–882.

8 G.-H. Kim, F. P. García de Arquer, Y. J. Yoon, X. Lan, M. Liu, O. Voznyy, Z. Yang, F. Fan, A. H. Ip, P. Kanjanaboos, S. Hoogland, J. Y. Kim and E. H. Sargent, *Nano Lett.*, 2015, **15**, 7691–7696.

9 P. K. Jain, X. Huang, I. H. El-Sayed and M. A. El-Sayed, *Acc. Chem. Res.*, 2008, **41**, 1578–1586.

10 P. Moroz, G. Liyanage, N. N. Kholmicheva, S. Yakunin, U. Rijal, P. Uprety, E. Bastola, B. Mellott, K. Subedi, L. Sun, M. V. Kovalenko and M. Zamkov, *Chem. Mater.*, 2014, **26**, 4256–4264.

11 M. V. Kovalenko, R. D. Schaller, D. Jarzab, M. A. Loi and D. V. Talapin, *J. Am. Chem. Soc.*, 2012, **134**, 2457–2460.

12 Z. Han, F. Qiu, R. Eisenberg, P. L. Holland and T. D. Krauss, *Science*, 2012, **338**, 1321–1324.

13 D. B. Khadka and J. Kim, *J. Phys. Chem. C*, 2014, **118**, 14227–14237.

14 T. K. Todorov, K. B. Reuter and D. B. Mitzi, *Adv. Mater.*, 2010, **22**, E150–E159.

15 P. S. Vasekar, T. P. Dhakal, Thin Film Solar Cells Using Earth-Abundant Materials, *Solar cells – research and application perspectives*, ed. A. Morales-Acevedo, InTech, 2013, p. 386, ISBN: 978-953-51-1003-3, DOI: 10.5772/3418.

16 P. R. Bonneau, R. F. Jarvis and R. B. Kaner, *Nature*, 1991, **349**, 510–512.

17 T. A. Bither, C. T. Prewitt, J. L. Gillson, P. E. Bierstedt, R. B. Flippen and H. S. Young, *Solid State Commun.*, 1966, **4**, 533–535.

18 J. G. Brennan, T. Siegrist, Y. U. Kwon, S. M. Stuczynski and M. L. Steigerwald, *J. Am. Chem. Soc.*, 1992, **114**, 10334–10338.

19 J.-P. Ge and Y.-D. Li, *J. Mater. Chem.*, 2003, **13**, 911–915.

20 M. Bochmann, *Chem. Vap. Deposition*, 1996, **2**, 85–96.

21 A. Sobhani and M. Salavati-Niasari, *J. Alloys Compd.*, 2015, **625**, 26–33.

22 W. Shi, X. Zhang, G. Che, W. Fan and C. Liu, *Chem. Eng. J.*, 2013, **215–216**, 508–516.

23 A. Liu, X. Chen, Z. Zhang, Y. Jiang and C. Shi, *Solid State Commun.*, 2006, **138**, 538–541.

24 B. Yuan, X. Hou, Y. Han, W. Luan and S.-T. Tu, *New J. Chem.*, 2012, **36**, 2101–2105.

25 M. Limpinsel, N. Farhi, N. Berry, J. Lindemuth, C. L. Perkins, Q. Lin and M. Law, *Energy Environ. Sci.*, 2014, **7**, 1974–1989.

26 M. Cabán-Acevedo, D. Liang, K. S. Chew, J. P. DeGrave, N. S. Kaiser and S. Jin, *ACS Nano*, 2013, **7**, 1731–1739.

27 T. Harada, *J. Phys. Soc. Jpn.*, 1998, **67**, 1352–1358.

28 L. Chun-Rong, Y.-J. Siao, S.-Z. Lu and G. Chie, *IEEE Trans. Magn.*, 2009, **45**, 4275–4278.

29 V. K. Gudelli, V. Kanchana, G. Vaitheeswaran, M. C. Valsakumar and S. D. Mahanti, *RSC Adv.*, 2014, **4**, 9424–9431.

30 F. Liu, J. Zhu, L. Hu, B. Zhang, J. Yao, M. K. Nazeeruddin, M. Gratzel and S. Dai, *J. Mater. Chem. A*, 2015, **3**, 6315–6323.

31 W. Wang, X. Pan, W. Liu, B. Zhang, H. Chen, X. Fang, J. Yao and S. Dai, *Chem. Commun.*, 2014, **50**, 2618–2620.

32 J. Li, Z. Jin, T. Liu, J. Wang, X. Zheng and J. Lai, *CrystEngComm*, 2014, **16**, 6819–6822.

33 Z. Qin, B. C. Yang, S. R. Zhang, K. Li, S. Q. Yan, X. W. Lv and Z. J. Li, *Vacuum*, 2015, **111**, 157–159.

34 W. Chengrong, B. Yongxiao, D. Aiying and B. Yan, *Nanotechnology*, 2016, **27**, 165702.

35 K. D. Oyler, X. Ke, I. T. Sines, P. Schiffer and R. E. Schaak, *Chem. Mater.*, 2009, **21**, 3655–3661.

36 W. Zhang, Y. Cheng, J. Zhan, W. Yu, L. Yang, L. Chen and Y. Qian, *Mater. Sci. Eng., B*, 2001, **79**, 244–246.

37 K. P. Bhandari, P. J. Roland, T. Kinner, Y. Cao, H. Choi, S. Jeong and R. J. Ellingson, *J. Mater. Chem. A*, 2015, **3**, 6853–6861.

38 T. Kinner, K. P. Bhandari, E. Bastola, B. M. Monahan, N. O. Haugen, P. J. Roland, T. P. Bigioni and R. J. Ellingson, *J. Phys. Chem. C*, 2016, **120**, 5706–5713.

39 J. Pickardt, B. Reuter, E. Riedel and J. Söchtig, *J. Solid State Chem.*, 1975, **15**, 366–368.

40 S. Tengner, *J. Inorg. Gen. Chem.*, 1938, **239**, 126–132.

41 S. Mourdikoudis and L. M. Liz-Marzán, *Chem. Mater.*, 2013, **25**, 1465–1476.

42 J. Zimdars and M. Bredol, *New J. Chem.*, 2016, **40**, 1137–1142.

43 W. Zhang, Z. Yang, J. Zhan, L. Yang, W. Yu, G. Zhou and Y. Qian, *Mater. Lett.*, 2001, **47**, 367–370.

44 H. D. Lutz and B. Müller, *Phys. Chem. Miner.*, 1991, **18**, 265–268.

45 B. Ganga, C. Ganeshraj, A. G. Krishna and P. Santhosh, arXiv preprint arXiv:1303.1381, 2013.

46 B. Ouertani, J. Ouerfelli, M. Saadoun, M. Zribi, M. B. Rabha, B. Bessaïs and H. Ezzaouia, *Thin Solid Films*, 2006, **511–512**, 457–462.

47 N. Hamdadou, A. Khelil, M. Morsli and J. C. Bernàde, *Vacuum*, 2005, **77**, 151–156.

48 D. Sharma, B. Joshi, K. Patel, V. Ganeshan and Y. Sharma, *International Journal of Recent Research and Review*, 2013, **6**, 32–49.

49 *Non-Tetrahedrally Bonded Binary Compounds II*, ed. O. Madelung, U. Rössler and M. Schulz, Springer Berlin Heidelberg, Berlin, Heidelberg, 2000, pp. 1–3, DOI: 10.1007/10681735_558.

50 *Non-Tetrahedrally Bonded Binary Compounds II*, ed. O. Madelung, U. Rössler and M. Schulz, Springer Berlin Heidelberg, Berlin, Heidelberg, 2000, pp. 1–3, DOI: 10.1007/10681735_560.